

Neuron, Volume 77

Supplemental Information

Local and Global Contrast Adaptation

in Retinal Ganglion Cells

Mona M. Garvert and Tim Gollisch

Inventory:

- Supplemental Figure S1 (related to Figure 2)
- Supplemental Figure S2 (related to Figure 3)
- Supplemental Text: Derivation of firing transients after switches in stimulus location
- Supplemental Experimental Procedures

Supplemental Figure S1

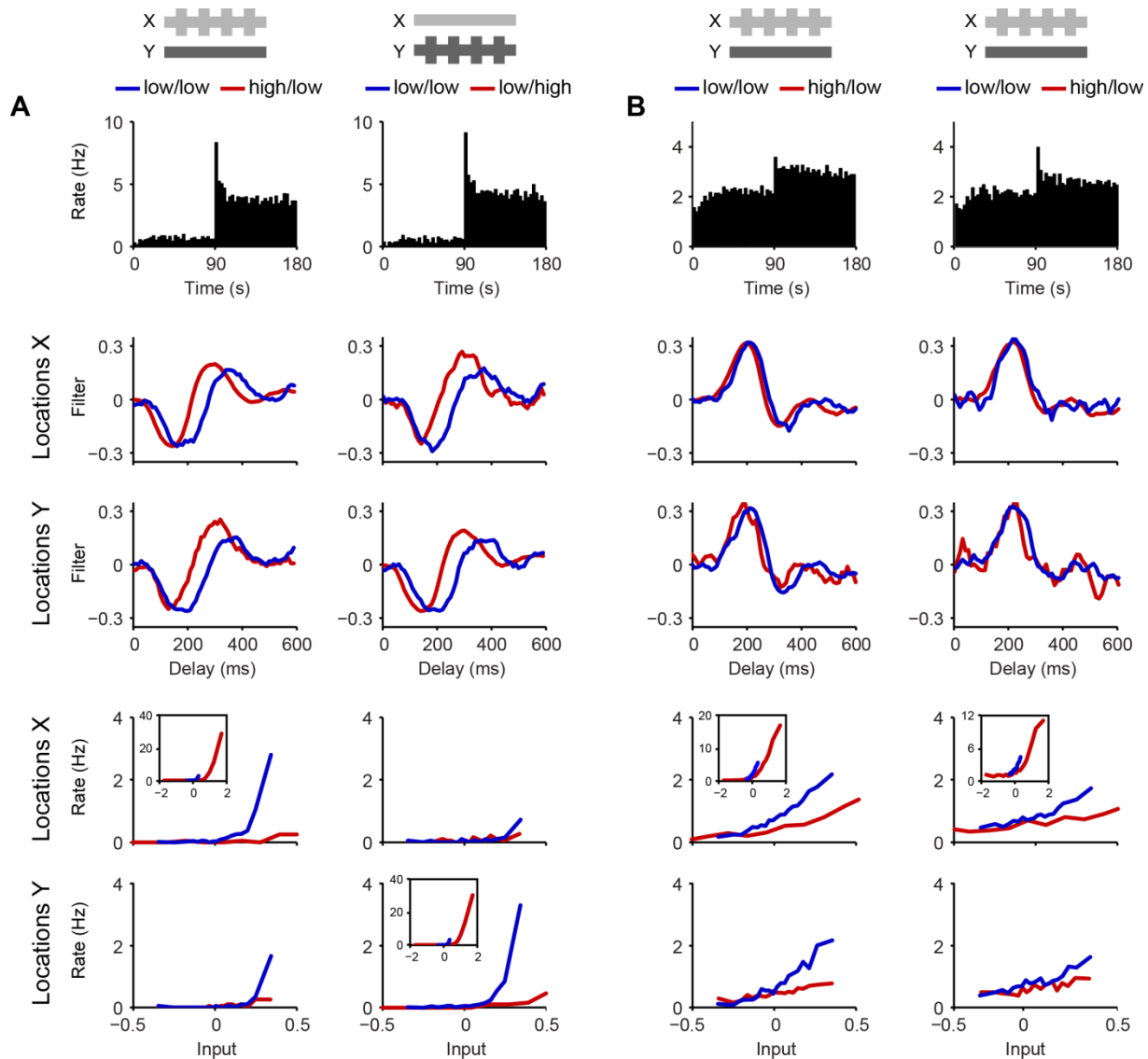


Figure S1 (related to Figure 2). Filters and nonlinearities under local contrast changes at either X or Y and from sample On cells

(A) Adaptation characteristics of an Off-type ganglion cell for local contrast changes at either X (left column) or Y (right column), presented analogously to the data of Figure 2. The data show that, when locations Y are used for the local contrast change instead of locations X, the local changes in the filters are interchanged between X and Y. In particular, the early filter parts are more similar and the change in the biphasic shape more pronounced at those locations where contrast does not change.

(B) Adaptation characteristics of two representative On-type ganglion cells for local contrast changes at X, presented analogously to the data of Figure 2. Contrast adaptation effects are weaker than typically observed for Off-type cells, and filter shapes hardly change. Sensitivity changes are more pronounced and consistent with a global scope of contrast adaptation, showing similar adaptation effects for X and Y.

Supplemental Figure S2

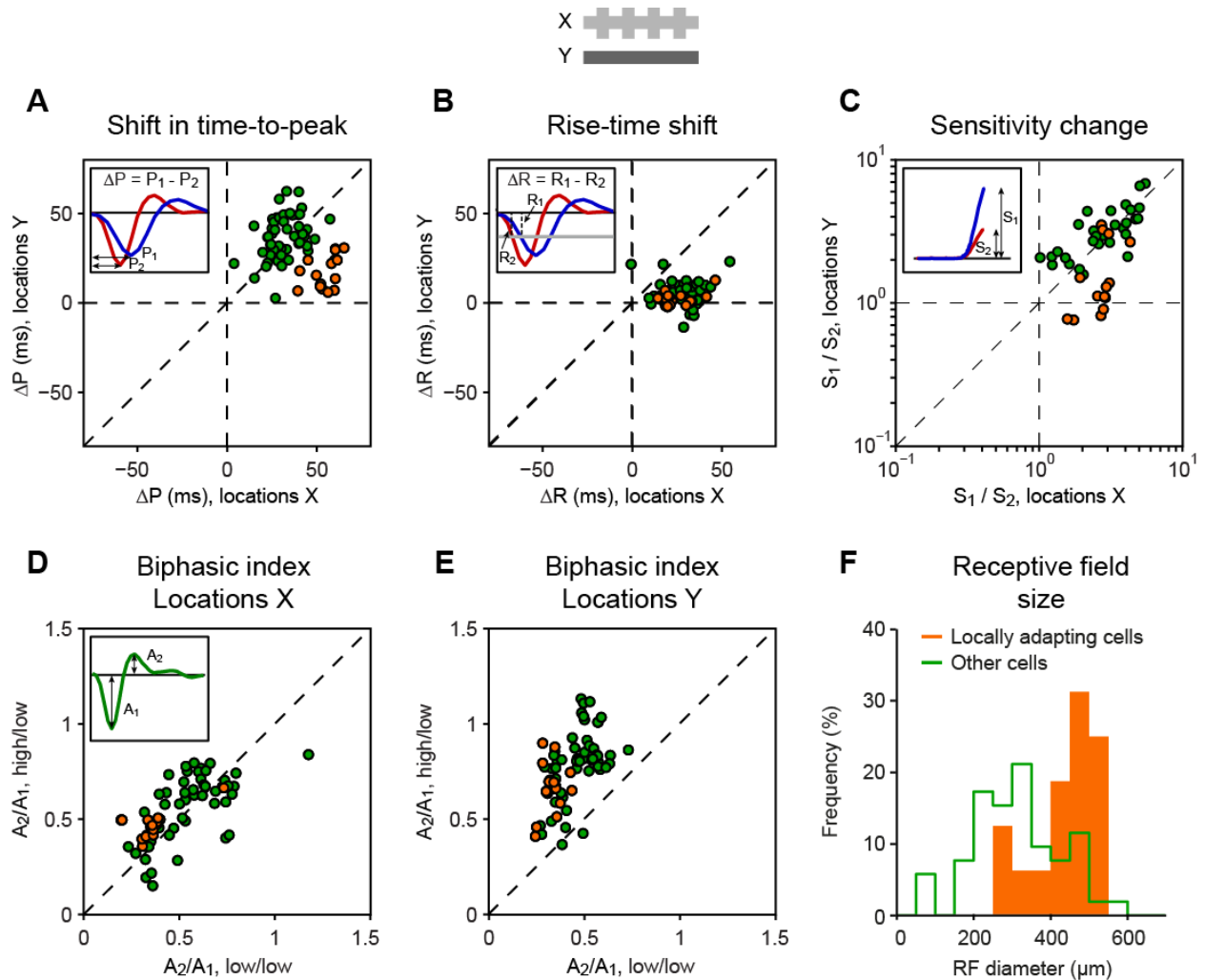


Figure S2 (related to Figure 3). Characterization of cells with local adaptation effects.

(A-E) Same data as presented in Figure 3, but with those cells labeled orange that had a significantly stronger shift in time-to-peak (panel A) for locations X as compared to locations Y (N=16 out of a total of 68 cells). The cells of this subgroup also typically had much weaker sensitivity changes for locations Y (panel C). Regarding changes in the biphasic shape of the filters (panels D and E), locally adapting cells had similar changes as other cells, but started from a lower baseline of biphasic indices, indicating that these cells tended to have more monophasic filter shapes.

(F) Histograms of receptive field sizes between locally adapting cells and other cells. Locally adapting cells generally had larger receptive fields than the remaining cells.

Supplemental Text

Derivation of firing transients after switches in stimulus location

We here analytically evaluate the model of Figure 8A in order to better understand the firing rate transients that occur in response to switches of stimulus location. To do so, we compare the average firing rate just after the switch, R_{switch} , to the average firing rate in the absence of a switch, R_{baseline} , when only one input channel provides signals. Let us assume that the stimulus is Gaussian white noise, sampled in discrete time steps, with standard deviation σ and that the temporal filter applied at each input channel is, for simplicity, power-normalized to unity. The latter just means that the filtered signal s that forms the output of one channel follows a Gaussian distribution with the same standard deviation σ as the stimulus.

Let us denote the nonlinearity that follows after the temporal filter by $F(s)$. The average firing rate R_{baseline} is then obtained by integrating $F(s)$ over the probability distribution of s :

$$R_{\text{baseline}} = \int_{-\infty}^{\infty} ds \frac{1}{\sqrt{2\pi\sigma^2}} e^{-\frac{s^2}{2\sigma^2}} F(s) \quad (1)$$

This has to be compared to the firing rate R_{switch} just after a switch in stimulus location when the signals from both input channels contribute according to their overlap with the temporal filter, as shown in Figure 8C. The filtered signals s_X and s_Y for the two inputs X and Y, respectively, are independent random variables that follow Gaussian distributions. The total variance σ^2 of the filter output is now distributed over these two channels, so that their variances σ_X^2 and σ_Y^2 sum to σ^2 . For the corresponding firing rate, we find

$$R_{\text{switch}} = \int_{-\infty}^{\infty} ds_X \frac{1}{\sqrt{2\pi\sigma_X^2}} e^{-\frac{s_X^2}{2\sigma_X^2}} F(s_X) + \int_{-\infty}^{\infty} ds_Y \frac{1}{\sqrt{2\pi\sigma_Y^2}} e^{-\frac{s_Y^2}{2\sigma_Y^2}} F(s_Y) \quad (2)$$

Note that the integrals in Eq. (2) have the same form as Eq. (1); only the variance of the Gaussian weighting functions are different. Whether R_{switch} is larger, smaller, or the same compared to R_{baseline} therefore depends on whether having contributions from two input channels outweighs the reduction in variance for the individual input signal. We can easily check this for particular cases:

1) If the nonlinearity is the threshold-linear function used in Figure 8 (i.e., $F(s) = s$ for $s > 0$ and $F(s) = 0$ otherwise), the integrals are proportional to the standard deviation of the Gaussian weighting functions (with some proportionality factor c). Thus $R_{\text{switch}} = c(\sigma_X + \sigma_Y)$

and $R_{\text{baseline}} = c\sigma = c\sqrt{\sigma_X^2 + \sigma_Y^2}$, and we find that $R_{\text{switch}} > R_{\text{baseline}}$ because

$\sigma_X + \sigma_Y > \sqrt{\sigma_X^2 + \sigma_Y^2}$, as can easily be seen by squaring both sides and noting that the variances are larger than zero. Therefore, the effect of having two input channels weighs more strongly than having reduced variance per input channel in this case. The maximal effect occurs when both input channels contribute equally, i.e., $\sigma_X = \sigma_Y$. For the peak size in the firing rate histogram, we then obtain $R_{\text{switch}} = \sqrt{2} R_{\text{baseline}}$. This is the case in the simulation of Figure 8B. In more realistic scenarios, however, the relation between peak size and baseline will be distorted by an additional output nonlinearity after summation of the two input channels. The output nonlinearity can boost the difference (if it is an accelerating nonlinearity) or diminish it (if it is a squashing nonlinearity), but typically not reverse the sign of the firing rate transient, at least as long as the output nonlinearity is monotonic.

2) If the nonlinearity is a threshold-quadratic or just a quadratic function, the integrals are proportional to the variance of the Gaussian weighting functions. In this case, the effect of having two input channels simply cancels the effect that each channel has reduced variance. Therefore, no firing rate peak will occur in the model in response to a switch in stimulus location.

3) More generally, if the nonlinearity is a threshold-power-law function with a power $n \in \{1, 2, \dots\}$ (i.e., $F(s) = s^n$ for $s > 0$ and $F(s) = 0$ otherwise), the integrals will be proportional to the n -th power of the standard deviation. Again, the maximal effect will (for symmetry reasons) occur when both input channels provide equal contributions, i.e., $\sigma_X = \sigma_Y = \frac{1}{\sqrt{2}}\sigma$. For this case, we have $\sigma_X^n + \sigma_Y^n = 2\left(\frac{1}{\sqrt{2}}\right)^n \sigma^n = 2^{\frac{2-n}{2}} \sigma^n$. We thus find (besides the relations derived above for $n = 1$ and $n = 2$) that for $n > 2$, $\sigma_X^n + \sigma_Y^n < \sigma^n$ so that the decreased variance in the individual inputs has a stronger effect than having two input channels. This means that the firing rate will transiently decrease in such a model when the stimulus location is switched.

Supplemental Experimental Procedures

Electrophysiology

Retinas were obtained from dark-adapted axolotl salamanders (*Ambystoma mexicanum*; pigmented wild type) of either sex. After enucleation of the eyes, the eyeball was hemisected and cornea, lens, and vitreous were removed from the eyeball to isolate the retina. The retina was separated from the pigment epithelium and cut in half. One half was placed on a multielectrode array (Multichannel Systems, 60 channels, 10- μm electrode diameter, 100- μm spacing) with the ganglion cell layer facing down. Pieces of retina that were not immediately used were stored in oxygenated, cooled Ringer's solution (110 mM NaCl, 2.5 mM KCl, 1.6 mM MgCl_2 , 1 mM CaCl_2 , 22 mM NaHCO_3 and 10 mM D-glucose, equilibrated with 95% O_2 and 5% CO_2) for later recordings. The dissection was performed with infrared illumination under a stereomicroscope equipped with night-vision goggles.

During recordings, the retina was continuously perfused with Ringer's solution at room temperature (20°C-22°C). The signals were amplified, band-pass filtered between 300 Hz and 5 kHz, and stored digitally at 25-kHz sampling rate. Spike sorting was performed with a custom-made software program, based on a Gaussian mixture model and an expectation-maximization algorithm (Pouzat et al., 2002). Only well-separated units with a clear refractory period were included in the analysis, totaling 68 ganglion cells from 9 retinas. In experiments with pharmacologically blocked inhibition, strychnine (5 μM), picrotoxin (150 μM), and bicuculline (20 μM) were added to the Ringer's solution, and recordings were resumed after 20 minutes incubation time.

Visual stimulation

Visual stimuli were displayed on a gamma-corrected cathode ray tube monitor with a refresh rate of 100 Hz, controlled through custom-made software based on Visual C++ and OpenGL. The image was projected onto the photoreceptor layer of the retina with each pixel on the monitor demagnified to 6 μm x 6 μm . Stimuli were presented on a gray background in the photopic range of either 5.1 mW/m^2 or 9.3 mW/m^2 with no difference in results.

For assessing the effects of contrast adaptation, we used random binary flicker of light intensity, drawn independently every 30 ms for each of the two sets of locations, X and Y. Each binary

intensity distribution had a high and a low intensity value, I_{high} and I_{low} , respectively, which occurred with equal probability. The high and low contrast conditions had contrast values $(I_{\text{high}} - I_{\text{low}}) / (I_{\text{high}} + I_{\text{low}})$ of 0.97 and 0.2, respectively, while keeping the same mean intensity $(I_{\text{high}} + I_{\text{low}}) / 2$, which was equal to the background intensity for each experiment. The different contrast conditions were presented in alternating trials of 90 seconds each, with the random sequences differing between trials. Overall recording times ranged from 40 to 60 min for each measurement of two alternating contrast conditions.

Receptive fields

We characterized the recorded ganglion cells as either On-type or Off-type and determined their spatial receptive fields with spike-triggered-average analysis (Chichilnisky, 2001), based on responses to a spatially uniform Gaussian white-noise stimulus and to a spatio-temporal binary white-noise stimulus on a checkerboard layout with subfields of $90 \mu\text{m} \times 90 \mu\text{m}$. To determine receptive field sizes, the spike-triggered-average obtained from spatio-temporal stimulation was separated into a spatial and a temporal component by a singular-value decomposition (Gauthier et al., 2009). The spatial component was fitted by a two-dimensional Gaussian function, from which the area A contained within the one-sigma contour was calculated. The receptive field diameter was then determined as $2\sqrt{A/\pi}$.

Analysis of filters and conditional nonlinearities

To calculate filters in response to the random binary stimulus sequences for each contrast condition, spike trains and stimuli were binned with a resolution of 10 ms. We then calculated the spatio-temporal filter as the spike-triggered average for the 600-ms period preceding a spike. Note that, despite the fact that the binary stimulus does not follow a spherically symmetric distribution, spike-triggered analysis is applicable to our data because the filters are much longer than the update time of the stimulus, so that the central limit theorem implies that stimulus projections onto relevant filters adhere to a symmetric, Gaussian distribution (Chichilnisky, 2001).

In the present case, the spike-triggered average corresponds to a 2×60 matrix, spanned by the 2 spatial components X and Y and 60 temporal components. Conceptually, this is equivalent to computing a spatio-temporal receptive field from responses to a flickering checkerboard pattern

(Chichilnisky, 2001), except for the smaller number of spatial components used in the present case. For display purposes and further analyses, we considered this spatio-temporal filter as a composition of two temporal filters for X and Y, respectively, whose contributions are summed, providing a mathematically equivalent description. For comparison of filter shapes, each temporal filter was normalized so that the sum of squares equaled unity. Note that the calculation of the spatio-temporal filter as the spatio-temporal spike-triggered average is equivalent to separately calculating the two purely temporal spike-triggered averages for X and Y, respectively, because the stimulus sequences at X and Y are independent. Thus, the perhaps counterintuitive identification of two temporal filters from a single spike train rests on the fact that these two temporal filters actually compose a single spatio-temporal filter.

The conditional nonlinearities were determined by a histogram method. To do so, stimuli were first convolved with the respective temporal filters to obtain the generator signals for both X and Y. Because of the normalization of the filters, the obtained generator signals had a standard deviation equal to the contrast of the corresponding stimulus component. The nonlinearities were then obtained by binning the generator signals of either X or Y, considering only those stimulus segments for which the generator signal from the other locations fell within the range $\pm 0.3 \times \text{contrast}$. For the histograms, we used 20 bins, which were spaced so that each contained approximately the same number of data points, and plotted the average generator signal against the average spike rate for each bin.

We computed a sensitivity measure S for each cell at both X and Y and for both contrast conditions by determining the maximum spike rate in the conditional nonlinearities over the input range spanned by the low-contrast condition. For low-contrast stimuli, this was just the spike rate in the last bin of the histogram, corresponding to the largest binned generator signal. For the high-contrast stimuli at the same location, we determined the spike rate that corresponded to the same generator signal as in the low-contrast condition by linearly interpolating the high-contrast histogram values. For cells with low firing rates, estimation of the nonlinearity for low-contrast stimulus components suffers from noise, resulting in unreliable sensitivity ratios. To minimize the effect of this noise on the population analyses (Figures 3C and 5C), we only included cells here for which all four sensitivity measures for the two locations and the two contrast conditions reached at least a value of 0.5 Hz. This excluded 25 of the 68 cells in Figure 3C and 30 of the 68 cells in Figure 5C.

We analyzed the response speed and biphasic nature of the temporal filters in the following way: To find the times and amplitudes of the first and second peak in the filter, we first smoothed each filter by convolution with a Gaussian of 10-ms standard deviation and then identified the filter sample points with maximal and minimal value and fitted second-order polynomials in the range ± 30 ms around these sample points. We determined the time-to-peak (Figures 3A and 5A) from the fit as the time of the first (negative) peak in the filter. To analyze how biphasic the filters were (Figures 3D-E and 5D-E), we used the fits to determine the absolute amplitude values A_1 and A_2 of the first (negative) and the second (positive) peak in the filter, respectively. The biphasic index (Zaghloul et al., 2007) was then computed as A_2/A_1 . We checked the robustness of this measure by repeating the analysis with and without prior smoothing of the filters and using different temporal ranges (stretching from ± 10 ms to ± 50 ms) for fitting polynomials around the extreme filter values or taking just the extreme values themselves. None of these variations had a substantial effect on the results, showing that the applied method yields a robust assessment of the biphasic shape of the filters. To analyze the kinetics of the early filter part, we computed the rise time (Figures 3B and 5B) by using linear interpolation to determine the time when the filter first crossed a threshold of -0.1 from above. This threshold was chosen to lie close to half-maximum for most filters.

Statistical analysis

We assessed statistical significance of the various contrast adaptation effects at both the population level as well as for each individual cell with nonparametric statistical tests, because several of the extracted measures for describing filter shapes and sensitivity did not follow normal distributions, as assessed by a Shapiro-Wilk test. At the population level, changes in filter shapes and sensitivity were statistically tested by Wilcoxon signed rank tests with a 5% significance criterion. This was used to assess changes between contrast conditions for either locations X and Y as well as differences in magnitude of these changes between X and Y.

To test specifically for a difference between the change in biphasicness at locations X and Y (Figures 3D and 3E), we calculated for each cell and both X and Y the ratio of the biphasic indices for the high/low and the low/low condition. The differences between X and Y in these ratios of biphasic indices were then tested by a Wilcoxon signed rank test. To test for local sensitivity changes in the experiment where global contrast stayed constant (Figure 5C), we divided the sensitivity ratio S_1/S_2 for locations X by the sensitivity ratio S_1/S_2 for locations Y, thus

obtaining $\frac{S_1(X)}{S_2(X)} / \frac{S_1(Y)}{S_2(Y)}$. This measures the increase in sensitivity at X when switching from

the high/low condition (index 2) to the low/high condition (index 1) relative to the sensitivity change at Y. This relative sensitivity measure has the advantage that – unlike the individual tests for sensitivity changes at either X or Y – it is relatively insensitive to global fluctuations in sensitivity between the two contrast conditions, which result from residual differences in global contrast over individual receptive fields when switching between the low/high and the high/low condition. The fact that the data points in Figure 5C lie mostly below the identity line indicates that the above ratio is mostly larger than unity and thus that there is a relative increase in sensitivity at X for the low/high condition. (In fact, the logarithm of this ratio is proportional to the distance of the data points from the identity line in the logarithmic plot of Figure 5C.) We tested whether this ratio deviated significantly from unity on the population level with a Wilcoxon signed rank test. For an alternative view of this measure, note that it can equivalently be written as

$\frac{S_1(X)}{S_1(Y)} / \frac{S_2(X)}{S_2(Y)}$. In this form, it can easily be interpreted as a measure of how the relative

sensitivity at X compared to Y changes when switching between the contrast conditions. Thus, the fact that this measure is larger than unity shows that relative sensitivity shifts towards a preference for X during the low/high condition and towards a preference for Y during the high/low condition.

To analyze statistical significance on a single-cell level, the recordings were divided into non-overlapping 10-second fragments. For each contrast condition, the fragments were randomly assigned to one of eight groups so that each group contained the same number of fragments. STAs were then calculated for each group separately and analyzed in the same fashion as described above to determine time-to-peak, rise time, and biphasic index, resulting for each of these measures in eight independent values for each contrast condition. To reduce the effect of occasional noise peaks that were bigger than the actual filter peaks of interest, fragment groups for which the detected peak differed by more than 80 ms from the original peak time were discarded together with their counterparts from the other stimulus condition. The sets of values obtained from the fragment groups were then used to test for statistical significance of changes between the two contrast conditions at the 5%-level using two-tailed Wilcoxon rank sum tests. For statistically testing which cells had a stronger shift in time-to-peak for locations X as compared to locations Y, a one-tailed Wilcoxon rank sum test was used. Changes in sensitivity were tested for statistical significance only on the population level, but not on the level of

individual cells because often the available data were insufficient to calculate conditional nonlinearities for the individual data fragments.

Modeling

For the models used in Figures 7 and 8, we used independent Gaussian white noise sequences with unit variance, sampled in discrete time steps Δt , as input signals at either X, Y, or both. Temporal filtering was applied by convolving the input sequences with the Off-type temporal filter $f(t) = c \left[\exp(-t^2 / 3^2) - \exp(-t^2 / 6^2) \right]$ for $t > 0$, with time measured in units of Δt and c used to normalize the filter to unit power. The filter shape is displayed in the corresponding boxes of Figures 7A and 8A. Rectification by the threshold-linear function at the corresponding stages was obtained by setting all negative values to zero. The feedback in Figure 7 was modeled by convolving the signal after the first rectification stage by an exponential function $g(t) = 0.6 \exp(-t / 3)$ for $t > 0$ and subtracting the result of the convolution from the original signal.

Supplemental References

Chichilnisky, E.J. (2001). A simple white noise analysis of neuronal light responses. *Network* 12, 199-213.

Gauthier, J.L., Field, G.D., Sher, A., Greschner, M., Shlens, J., Litke, A.M., and Chichilnisky, E.J. (2009). Receptive fields in primate retina are coordinated to sample visual space more uniformly. *PLoS Biol* 7, e1000063.

Pouzat, C., Mazor, O., and Laurent, G. (2002). Using noise signature to optimize spike-sorting and to assess neuronal classification quality. *J Neurosci Methods* 122, 43-57.

Zaghloul, K.A., Manookin, M.B., Borghuis, B.G., Boahen, K., and Demb, J.B. (2007). Functional circuitry for peripheral suppression in Mammalian Y-type retinal ganglion cells. *J Neurophysiol* 97, 4327-4340.